

How quickly can sodium-ion learn? Assessing scenarios for techno-economic competitiveness against lithium-ion batteries

Adrian Yao^{1,3}, Sally M. Benson², and William C. Chueh^{*1,2,3}

¹Department of Materials Science & Engineering, Stanford University, Stanford, CA 94305, USA.

²Department of Energy Science & Engineering, Stanford University, Stanford, CA 94305, USA.

³Applied Energy Division, SLAC National Accelerator Laboratory, Menlo Park, CA 94025, USA.

ABSTRACT

Sodium-ion batteries have garnered significant attention as a potentially low-cost alternative to lithium-ion batteries, which have experienced supply shortages and pricing volatility of key minerals. Here we assess their techno-economic competitiveness against incumbent lithium-ion batteries using a modeling framework incorporating componential learning curves constrained by minerals prices and engineering design floors. We compare projected sodium-ion and lithium-ion price trends across over 6,000 scenarios while varying Na-ion technology development roadmaps, supply chain scenarios, market penetration, and learning rates. Assuming substantial progress can be made along technology roadmaps via targeted R&D, we forecast many sodium-ion pathways to be price competitive against low-cost lithium-ion variants in the early 2030s. Additionally, we show timelines are highly sensitive to movements in critical minerals supply chains—namely that of lithium, graphite, and nickel. Modeled outcomes suggest increasing sodium-ion energy densities to decrease materials intensity to be among the most impactful ways to improve competitiveness.

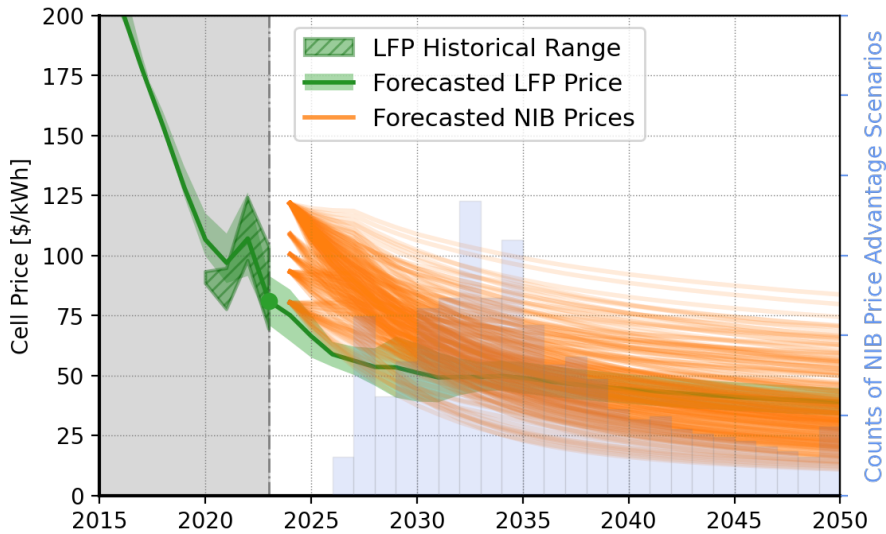


Figure 1: Forecasting Na-ion price curves against Li-ion (LFP) based on various technological, market, and supply chain conditions. A subset of the modeled price curves for Na-ion (orange) shown here against the forecasted LFP baseline. Histogram of complete set of modeled scenarios illustrates counts of modeled NIB scenarios with their respective Price Advantage years, suggesting many pathways to price competitiveness in the early 2030s.

* Corresponding Author. E-mail: wchueh@stanford.edu

The energy transition requires massive deployment of batteries for electric vehicles (EVs) and stationary energy storage systems (ESS). Lithium-ion (Li-ion) batteries have been responsible for nearly all new deployments of storage in recent years¹⁻³, largely enabled by the tremendous cost declines over the past three decades of commercialization characterized by an aggressive learning rate where prices have fallen by more than 97% since they were first commercialized in 1991^{4,5}. This trend is reflected in the average Li-ion cell prices shown in Supplementary Discussion 1 aggregated from the industry data contributors to this work^{1-3,6}, which also resolves the diverging price trajectories of NMC-type (nickel-manganese-cobalt oxide) and LFP-type (lithium iron phosphate) cathode chemistries. However, rapid Li-ion demand growth has recently placed a significant burden on the minerals supply chain—namely that of lithium, nickel, graphite, and cobalt—resulting in a first-ever increase in the average Li-ion cell price index in 2022³ which subsequently fell again as minerals prices plummeted⁷⁻⁹. This has prompted concerns regarding the overdependence on Li-ion and the susceptibility to production bottlenecks, supply chain shocks, and geopolitical constraints.

Sodium-ion (Na-ion) batteries present a potentially viable near-term substitute for Li-ion for two primary reasons: (1) increased abundance and availability of sodium suggests lower prices and (2) drop-in compatibility with Li-ion manufacturing infrastructure suggests rapid scaling timelines. Therefore, in response to severe post-COVID lithium price spikes, manufacturers recently announced over 240 GWh of Na-ion cell manufacturing pipeline through 2030¹⁰, promising lower prices than Li-ion. However, exactly if, when, and by how much Na-ion batteries will be price advantageous is still largely a matter of speculation.

Learning curves have been widely used in forecasting technological progress and price since patterns of improvement were first postulated by Wright for manufacturing airplanes¹¹. The typical learning curve (Wright's Law) predicts price reductions as a function of cumulative production ("learning-by-doing"), and has been statistically shown to produce accurate forecasts across wide-ranging sectors¹², including energy technologies¹³. Given the industrial importance of Li-ion batteries, several studies have sought to characterize their price trends using the conventional form of Wright's Law^{4,14-16} whereas others have ascribed additional descriptors, such as learning-by-researching or economies-of-scale, to understand their historic trends^{4,5,17}. However, conventional learning curves unrealistically assume infinite cost reductions approaching zero, which neglects limits set by underlying minerals. Therefore, yet other approaches have sought to additionally constrain the learning curve with a minerals price floor to produce more realistic projections¹⁸.

In this work, we propose an augmented learning curve model to better forecast future price trends by combining componential, floor-constrained learning curves for individual material components with technical development roadmaps that also exhibit learning behavior. We then use it to forecast battery price trends for Li-ion and Na-ion in various technological, market, and supply chain conditions to identify strategies that improve the techno-economic competitiveness of Na-ion (Figure 1).

Componential floor-constrained learning curves

We construct historical and forecasted aggregate price curves by incorporating knowledge of both (a) material component prices (in $\text{\$-kg}^{-1}$ or $\text{\$-m}^{-2}$) which evolve via learning-by-doing and (b) material component intensities (kg-kWh^{-1}) which evolve due to continued cell engineering and materials advancements—the latter of which has contributed greatly to Li-ion price declines to date^{4,5}. Here, we institute practical floors for both—using minerals price floors for the former and engineering limits for the latter. For each material component in a battery cell, we construct individual learning curves and institute a price floor based upon their underlying composition of benchmarkable key minerals which dynamically evolve with time. The learning curve that rides upon the minerals floor therefore represents the costs associated with chemical conversion. Each floor-constrained learning curve is then summed according to their mass- or areal-intensity per unit of stored energy content derived from detailed cell modeling.

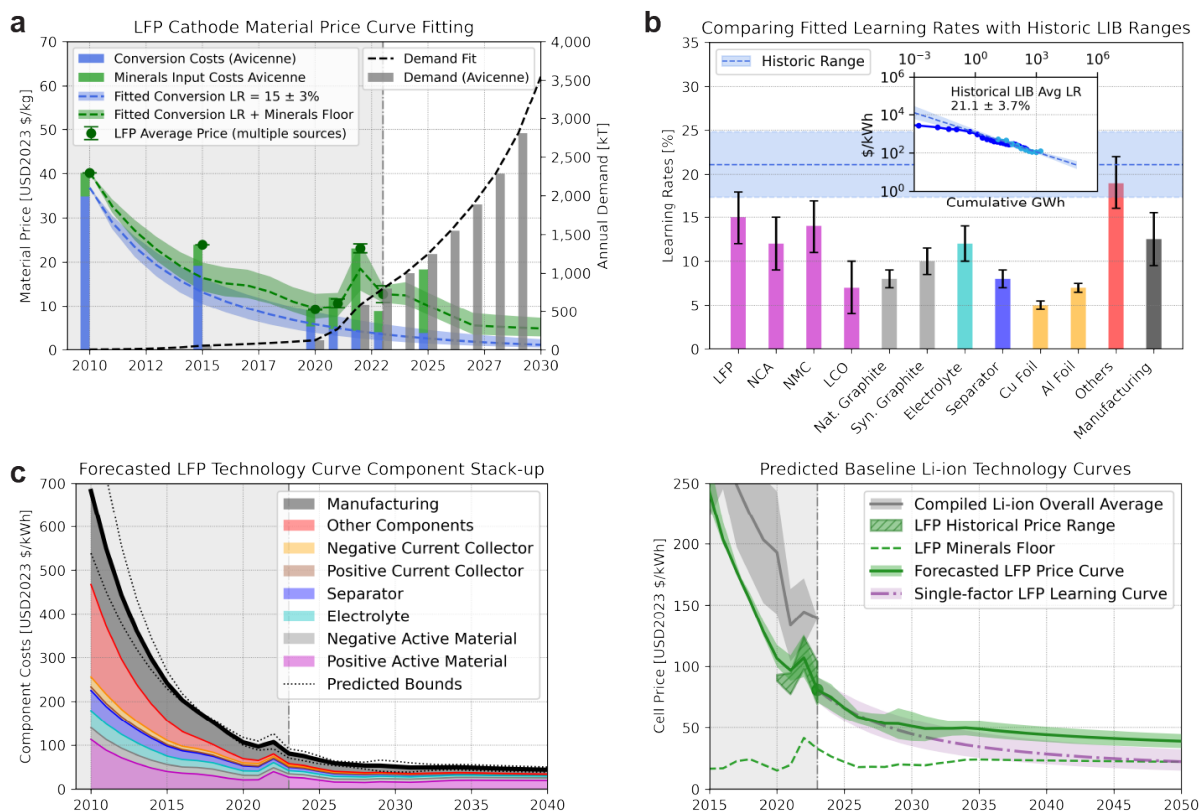


Figure 2: Componential floor-constrained construction of technology price curves. **a.** Example material component price curve generation for LFP material. A learning curve (in blue) is fit against historical conversion cost data to capture experience as cumulative production increases (gray bars and dotted black line) while a minerals price floor (in green) rides upon the learning curve. Reasonable agreement between the generated price curve and average prices collected from industry sources is observed. **b.** Fitted learning rates for key Li-ion material components (NCA=nickel-cobalt-aluminum oxide, LCO=lithium cobalt oxide, Nat. Graphite=natural graphite, Syn. Graphite=synthetic graphite) compared against the historical average learning rate (LR) for Li-ion compiled from literature and industry reports—shown in inset. See Supplementary Discussion 5 for details. **c.** Total price curve for LFP-type cells constructed by summing up all constituent material components based upon cell design models that inform materials intensity per energy content stored. See Supplementary Discussion 9 for equivalent plots for NMC. **d.** Forecasted LFP Li-ion price curve for the baseline scenario, showing good agreement with historical averages. A typical single-factor learning curve using the historical average learning rate (established in **b**) is also shown for comparison with potentially overly optimistic outcomes. Confidence intervals capture underlying uncertainty in minerals prices, starting materials prices, and learning rates.

We base our models upon a wide-ranging collection of sources obtained from industry data contributors to ensure accuracy and relevance. They include Benchmark Mineral Intelligence, Wood Mackenzie, BloombergNEF, Avicenne Energy, S&P Global, and other commercial reports^{19,20}. Additionally, we validate and confirm accuracy and relevance by surveying a panel of industry experts to obtain inputs on realistic price figures, state-of-art cell designs, and production costs²¹.

Establishing Li-ion baselines

We first obtain historical and forecasted minerals pricing for key commodities (lithium, nickel, cobalt, graphite, copper, manganese, aluminum, etc.) from industry sources^{1,2,22,23}. In all cases, historical prices were also collected from the United States Geological Survey (USGS) mineral commodity summaries dating back to 1991²⁴, and all price figures were inflation-adjusted to USD2023. Aggregated minerals prices are shown in Supplementary Discussion 2. As accurately predicting the future price movements of key

minerals is inherently challenging, we also separately model fixed-price high/mid/low forecasted scenarios to test sensitivity (see Supplementary Discussion 2.1). Based on the known elemental composition of each material component, we then calculate their price floors which evolve with minerals price movements (see Supplementary Discussion 3). For NMC-type materials that have historically experienced an evolution in stoichiometry, we take a volume-weighted average of each “nodal” composition to reflect a representative mix at every time step (see Supplementary Discussion 4).

To construct the baseline Li-ion price curves, we divide the effort into two parts: historical and forecasted, with the year 2023 designated present-day. We model both LFP- and NMC-type cells as a baseline but focus on LFP in the Main Text as it is widely considered the more relevant comparison with Na-ion with respect to performance and cost. Historical pricing of material components (in $\text{\$-kg}^{-1}$ or $\text{\$-m}^{-2}$ for mass- or areal-based components) were tabulated from industry and literature sources to establish a time series starting at or before 2010^{2,19,5,25,26}. Where available, information on chemical conversion costs were used to inform fitting. We also collected data on historical production quantities for each material to enable calculation of cumulative “experience” for each component. With knowledge of minerals price floors, historical component pricing, and cumulative production quantities, this leaves the learning rate as the only fitting parameter, per Equation (3) in Methods. To ensure continuity with forecasts, historical price curves were constrained to converge on present-day (2023) materials pricing, which were obtained from various industry sources and aggregated for robustness^{2,19,21,25,26}. An example price curve construction for LFP cathode material is shown in Figure 2a. The full set of fitted material price curves are presented in Supplementary Discussion 5, and their fitted learning rates are summarized in Figure 2b in comparison with average historical Li-ion learning rates aggregated from prior literature^{3,4,14,15,17}.

Having established historical component-specific learning rates and present-day prices, forecasted curves then depend on market growth rate assumptions and minerals price movements. Total battery market growth forecasts (in GWh) from several market intelligence sources were approximated with Gompertz functions to obtain continuous curves (see Methods and Supplementary Discussion 6). The three key market segments modeled were stationary ESS, two/three-wheelers and micromobility (TTW/MM), and EVs. Specifically, we consider three hypothetical Na-ion market growth scenarios with increasing degrees of penetration, ranging from the most conservative: 100% Na-ion penetration into ESS by 2040, to the most aggressive: 100% penetration into ESS by 2035, 100% of TTW/MM by 2040, and 25% EVs by 2040. Note that the most conservative market penetration scenario matches more closely to forecasts provided by industry data contributors. A “LIB Base Case” scenario was also modeled, which assumes no appreciable Na-ion deployment and a LFP market penetration scenario with 50% market share saturation reached by 2050 (see Supplementary Discussion 6.1). We use this for the baseline Li-ion price curve forecasts.

Combining compartmental learning with technology roadmaps

Forecasted price curves for each material component were then calculated using the same learning rates as their respective historical values. Subsequently, NMC and LFP cell designs were modeled based upon teardowns of state-of-art commercial cells published in literature^{27–29} (see Supplementary Discussion 7). Additionally, cell designs representing state-of-art in the past were also modeled from commercial cell teardowns in literature as well as industry reports documenting contemporaneous engineering progress at the time of their publication^{30–32}. This enabled fitting of materials intensity trends between past, present, and future that correspond with development roadmaps (see Supplementary Discussion 8). Finally, combining material component learning curves and materials intensity roadmaps, complete price curves were constructed as shown in Figure 2c for LFP (NMC component curve stack-up shown in Supplementary Discussion 9). The final LFP price curve is shown in Figure 2d with predicted prices reaching $\text{\$51 kWh}^{-1}$ by 2030, and the NMC price curve is shown to reach $\text{\$75 kWh}^{-1}$ in the same time frame (see Supplementary Discussion 9).

We emphasize that these forecasted cell prices include manufacturing overhead and profit. In reality, cell prices experience additional volatility in response to short-term market conditions. For example, recent announcements by major LFP incumbents indicated pricing at \$56 kWh⁻¹ in the latter half of 2024 (~2-3 years earlier than our forecasts, which reach \$56 kWh⁻¹ in 2027), largely seen as a strategy to maintain market share amid stagnating short-term EV sales³³ along with low short-term lithium prices—even lower than those forecasted in the baseline scenarios used here^{7,34}. These announcements validate that the aggressive prices derived from our modeling approach are in fact realizable before 2030.

A closer look at learning

Examining the fitted componential learning rates, learning rates appear correlated with processing complexity. Higher complexity processes (e.g. cathode synthesis, cell assembly) tend to have higher rates of learning whereas lower complexity processes (e.g. metal foil and anode production) tend to have lower rates (see Supplementary Discussion 5.2 for further discussion). However, in comparison to previous literature on Li-ion learning rates, we observe that our componential learning rates are all lower than the aggregate average rate experienced by historical cell prices (Figure 2b) of $21.1 \pm 3.7\%$ ^{3,4,14,15,17}, which suggests there must be another key contributor responsible for the aggressive price reductions in Li-ion. This can be explained by the technical advancements in the design of Li-ion cells over the past several decades, now requiring substantially lower materials intensity on a per-kWh basis than before^{4,5}. Specifically, the shift from cells optimized for power to those optimized for energy enabled higher active material utilization^{5,16,32}. The steady improvements to material specific capacities have also contributed to this phenomenon.

Therefore, the aggressive Li-ion price trends appears to be a story of modest price reductions in materials from learning-by-doing compounded by significant engineering advancements and learnings. This deconvolution of the traditional learning model into key constituent contributors is an important nuance to forecast realistic price trends of incumbent and emerging technologies like Li-ion and Na-ion, respectively. To illustrate, Figure 2d additionally compares price forecasts of LFP cells using our method—accounting for minerals price and engineering design floors—against the typical unconstrained single-factor learning curve form of Wright’s Law (Equation (1) in Methods) utilizing the historical average Li-ion rate. This curve nearly intersects the calculated LFP minerals price floor in 2050, which may be unrealistic and overly optimistic.

Forecasting Na-ion cell development roadmaps

Like Li-ion, Na-ion is an umbrella term encompassing several material chemistries generally categorized by cathode material classes. They include transition metal layered oxides, polyanions, and Prussian Blue analogues (PBAs)³⁵. Recent commercialization efforts indicate significant momentum behind (i) layered oxides with a general formula of Na_x(M)O₂ (x~1, M=Ni, Fe, Mn, Cu) with NaNi_xMn_y(M)_{1-x-y}O₂ (NaNM) being the most common and (ii) vanadium-free mixed-polyanions with the formula Na₄Fe₃(PO₄)₂(P₂O₇) (NFPP)²¹. In almost all instances, disordered hard carbons (HC) are used as Na-ion anode materials instead of the crystalline graphite used in Li-ion batteries due to their low sodium storage capacities³⁶. Alternative anodes to hard carbons include emerging technology directions such as (i) metallic tin (Sn) that alloys with sodium³⁷ or (ii) “anode-free” configurations that electrodeposit and strip sodium metal directly on current collectors^{38,39}. Here, in reference to NaNM, we specifically model NaNi_{0.33}Mn_x(M)_{0.67-x}O₂ where M includes Mg and Ti dopants and that are currently being commercialized⁴⁰⁻⁴². As the non-nickel transition metals contribute negligible minerals costs and redox activity⁴², our NaNM archetype also functionally represents compositions such as NaNi_{0.33}Fe_{0.33}Mn_{0.33}O₂ (NFM111). Given the recent interest in replacing nickel with earth-abundant elements like iron and manganese due high costs, we also model a material such as Na_{0.67}Fe_{0.5}Mn_{0.5}O₂ (NaFM). However, as these materials still suffer from unresolved performance challenges, we model technical roadmaps that gradually reduce nickel to 0% by ~2040 (see Supplementary

Discussion 10)—analogous to the gradual reduction of cobalt content in NMC cathodes over the years. This is modeled separately from roadmaps that maintain a static 33% nickel stoichiometry.

Given the importance of capturing engineering advancements on techno-economics, we model a multitude of Na-ion cell development roadmaps for NaNM|HC, NaFM|HC, NFPP|HC, NaNM|Sn, NaFM|Sn, NFPP|Sn, NaNM|Anode-free, and NaFM|Anode-free cell designs (see Supplementary Discussion 7 for details on 18 different Na-ion cell designs). These roadmaps assume gradual improvements from state-of-art 2024 designs toward future technical advancements by 2030 that increase energy densities and thereby reduce prices. See Methods and Supplementary Discussion 8 for details on fitting trends with a modified Moore’s Law. A summary of the modeled technical roadmaps is tabulated in Table 1.

Table 1: Summary of modeled Na-ion technical development roadmaps including gravimetric and volumetric energy densities (GED and VED) of modeled large-format pouch cells.

Roadmap Name	Starting Cell Design (2024)	Improved Cell Design (2030)	GED / VED [Wh/kg] / [Wh/L]	
			2024	2030
NaNM HC 0	NaNM HC Baseline	⇒ NaNM HC Baseline (No improvements)	134 / 272	
NaNM HC 1	NaNM HC Baseline	⇒ Increased electrode loadings	134 / 272	142 / 295
NaNM HC 2	NaNM HC Baseline	⇒ Anode capacity increase to 400 mAh-g ⁻¹	134 / 272	157 / 325
NaNM HC 3	NaNM HC Baseline	⇒ Cathode 20% capacity increase	134 / 272	160 / 314
NaNM HC 4	NaNM HC Baseline	⇒ Anode & cathode capacity increase	134 / 272	174 / 347
NaNM HC 5	NaNM HC 4.2V Baseline	⇒ Anode & cathode capacity increase @ 4.2V	134 / 272	196 / 376
NaNM HC 6	NaNM HC Baseline	⇒ Anode capacity increase to 400 mAh-g ⁻¹ @ 4.2V	134 / 272	181 / 359
NaNM HC 7	NaNM HC Baseline	⇒ Anode & cathode capacity increase @ 4.2V	155 / 303	196 / 376
NaFM HC 1	NaFM HC Baseline	⇒ Increased electrode loadings	134 / 272	142 / 295
NaFM HC 2	NaFM HC Baseline	⇒ Anode capacity increase to 400 mAh-g ⁻¹	134 / 272	157 / 325
NaFM HC 3	NaFM HC Baseline	⇒ Cathode 20% capacity increase	134 / 272	160 / 314
NaFM HC 4	NaFM HC Baseline	⇒ Anode & cathode capacity increase	134 / 272	174 / 347
NaFM HC 5	NaFM HC 4.2V Baseline	⇒ Anode & cathode capacity increase @ 4.2V	134 / 272	196 / 376
NaFM HC 6	NaFM HC Baseline	⇒ Anode capacity increase to 400 mAh-g ⁻¹ @ 4.2V	134 / 272	181 / 359
NaNM Sn 0	NaNM Sn Baseline	⇒ NaNM Sn Baseline (No improvements)	185 / 476	
NaNM Sn 1	NaNM Sn Baseline	⇒ Cathode 20% capacity increase	185 / 476	216 / 551
NaFM Sn 0	NaFM Sn Baseline	⇒ NaFM Sn Baseline (No improvements)	185 / 476	
NaFM Sn 1	NaFM Sn Baseline	⇒ Cathode 20% capacity increase	185 / 476	216 / 551
NFPP HC 0	NFPP HC Baseline	⇒ NFPP HC Baseline (No improvements)	111 / 210	
NFPP HC 1	NFPP HC Baseline	⇒ Increased electrode loadings	111 / 210	119 / 226
NFPP HC 2	NFPP HC Baseline	⇒ Anode capacity increase to 400 mAh-g ⁻¹	111 / 210	126 / 241
NFPP Sn 0	NFPP Sn Baseline	⇒ NFPP Sn Baseline (No improvements)	137 / 305	
NFPP Sn 1	NFPP Sn Baseline	⇒ Increased electrode loadings	137 / 305	147 / 330
NaNM AF 0	NaNM Anode-free Base.	⇒ NaNM Anode-free Baseline (No improvements)	207 / 547	
NaNM AF 1	NaNM Anode-free Base.	⇒ Increased electrode loadings	207 / 547	239 / 635

NaNM AF 2	NaNM Anode-free Base. ⇒	Cathode 20% capacity increase	207 / 547	283 / 734
NaFM AF 0	NaFM Anode-free Base. ⇒	NaFM Anode-free Baseline (No improvements)	207 / 547	
NaFM AF 1	NaFM Anode-free Base. ⇒	Cathode 20% capacity increase	207 / 547	283 / 734

Evaluating Roadmap “NaNM|HC 7” as an example: an NaNM|HC Baseline cell design (see Supplementary Discussion 7.7) evolves to experience an increase in hard carbon specific capacity from $330 \text{ mAh}\cdot\text{g}^{-1}$ to $400 \text{ mAh}\cdot\text{g}^{-1}$, an increase in cell operating voltage from 4.0 to 4.2V, and a 20% increase to NaNM specific capacity (to $\sim 175 \text{ mAh}\cdot\text{g}^{-1}$ measured from 2.0 to 4.25V) (see Supplementary Discussion 7.13)—all by 2030. The resulting materials intensity trends are shown in Figure 3a. Pricing for key Na-ion materials components are obtained by surveying industry expert sources to ensure commercial relevance²¹. These values are summarized in Figure 3b and further elaborated in Supplementary Discussion 11. Applying various learning rates and market growth assumptions, we forecast Na-ion price curves via our componential construction methodology. Figure 3c illustrates a scenario with the most conservative market penetration (100% Na-ion penetration into ESS by 2040, see Supplementary Discussion 6) and with novel cumulative experience applied to the anode material only (see Supplementary Discussion 12).

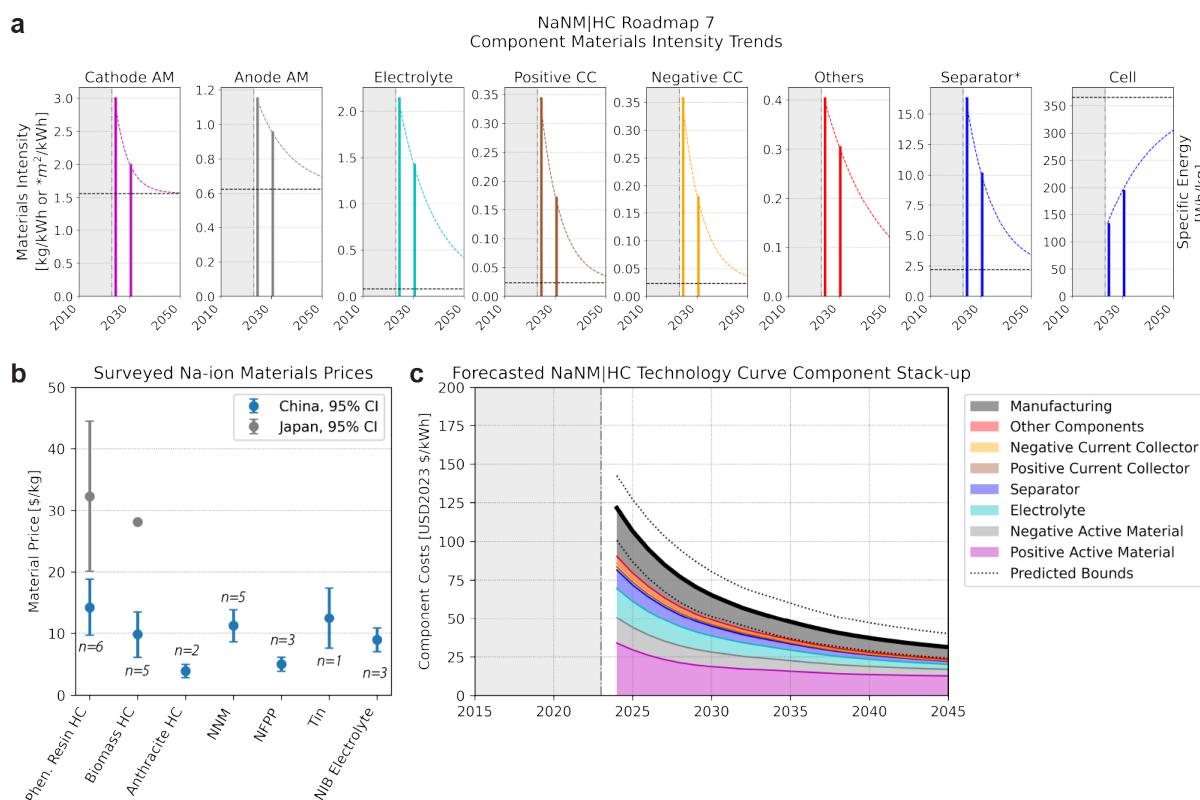


Figure 3: Exemplary Na-ion price curve construction based on cell modeling, road mapping, and realistic materials price assessments. **a.** Fitted materials intensity trends that approach asymptotic engineering floors (horizontal dashed lines), shown here for Roadmap “NaNM|HC 7”. AM=Active Material, CC=Current Collector. **b.** Surveyed price assessments for present-day Na-ion materials. The number of surveyed sources per material component (n) are also shown, and the 95% confidence interval indicates the high- and low-range estimates of prices. Note that each source may provide more than one value if also providing a range (see Supplementary Discussion 11). **c.** Componential construction of Na-ion price curve for given technical roadmap. Predicted bounds illustrate confidence intervals on the total curve from underlying uncertainty in minerals prices, starting materials prices, and learning rates.

It is worth highlighting our key assumptions. Here, we assume: (1) drop-in compatibility with existing Li-ion manufacturing infrastructure, which implies immediate high-yield production and no new manufacturing learnings (see Supplementary Discussion 12), (2) decoupled market penetration and technology pricing, whereby endogeneity captured within a typical demand curve is ignored for the sake of modeling and understanding intervention opportunities, and (3) transferable learning rates from Li-ion to Na-ion, where cathodes, anodes, and other components learn at their same respective rates between the two alkali chemistries. This last assumption may be supported by Supplementary Discussion 5.2, but more aggressive learning rates are also evaluated in our scenarios analysis below. We note that the first two assumptions enable a best-case scenario to model Na-ion's techno-economic competitiveness as a starting point. Additionally, we do not include next-generation Li-ion roadmaps (lithium manganese iron phosphate cathodes, silicon anodes, etc.) to again evaluate a best-case scenario for Na-ion. We finally emphasize that here we are only assessing the technologies at the cell-level with the price of stored energy ($\text{\$-kWh}^{-1}$) as the primary figure of merit. Therefore, this work does not capture systems-level considerations (e.g. potential savings on pack integration due to enhanced safety or reduced thermal management) or alternative performance-enabled economic considerations (e.g. potentially lower levelized price of storage due to increased cycle life). We address these additional complexities in future work.

Modeling scenarios to find conditions for competitiveness

Using the above approach, we evaluate 6,048 combinations of scenarios, all assuming GWh-scale production for Na-ion commences in 2024. The scenario variables evaluated are detailed in Supplementary Discussion 13. For each scenario, the Li-ion and Na-ion price curves are calculated and compared, producing plots exemplified by those shown in Figure 4a. This example illustrates a “NaFM|HC 2” roadmap where an initially 33% nickel stoichiometry cathode evolves to ~0% by 2040 while maintaining the same specific capacity, and a hard carbon anode evolves to increase its specific capacity to 400 mAh-g^{-1} by 2030. Due to the reduction in nickel content, the minerals price floor decreases substantially between 2024 and 2035.

Given that the forecasted curves carry uncertainty from confidence intervals of minerals prices (Supplementary Discussion 2), starting materials prices (see Figure 3b), and learning rates (see Figure 2b), we employ methods established in prior forecasting literature⁴³ to quantify expected timelines for price parity and advantage by calculating the probability at each time step that one technology is lower priced than the other. These probability plots are shown in the right-hand side of Figure 4a and Figure 4b comparing LFP against the modeled example Na-ion scenarios. We further define a “Price Parity” condition as the point in which Na-ion has $\geq 20\%$ probability of being lower priced than LFP, and a “Price Advantage” condition when that probability exceeds 80%. The yellow hatched regions in Figure 4a and Figure 4b therefore mark the periods in which a Na-ion technology and LFP are competitive in pricing and may be considered substitutes, performance notwithstanding.

Figure 4b models an identical set of assumptions as Figure 4a with the exception of a hypothetical graphite supply shock in 2027 that causes a permanent offset in prices but continues to learn at the same rate (see Supplementary Discussion 14 for details). This enables analysis of techno-economic competitiveness and risk considering potential supply chain disruptions. In the absence of a graphite supply shock condition as illustrated in Figure 4a, the Price Parity timeline is extended from 2032 to 2035, and the Price Advantage timeline is delayed substantially from 2038 to 2047. This large disparity is a result of the similar slopes of the price curves, which are nearly coinciding during this period.

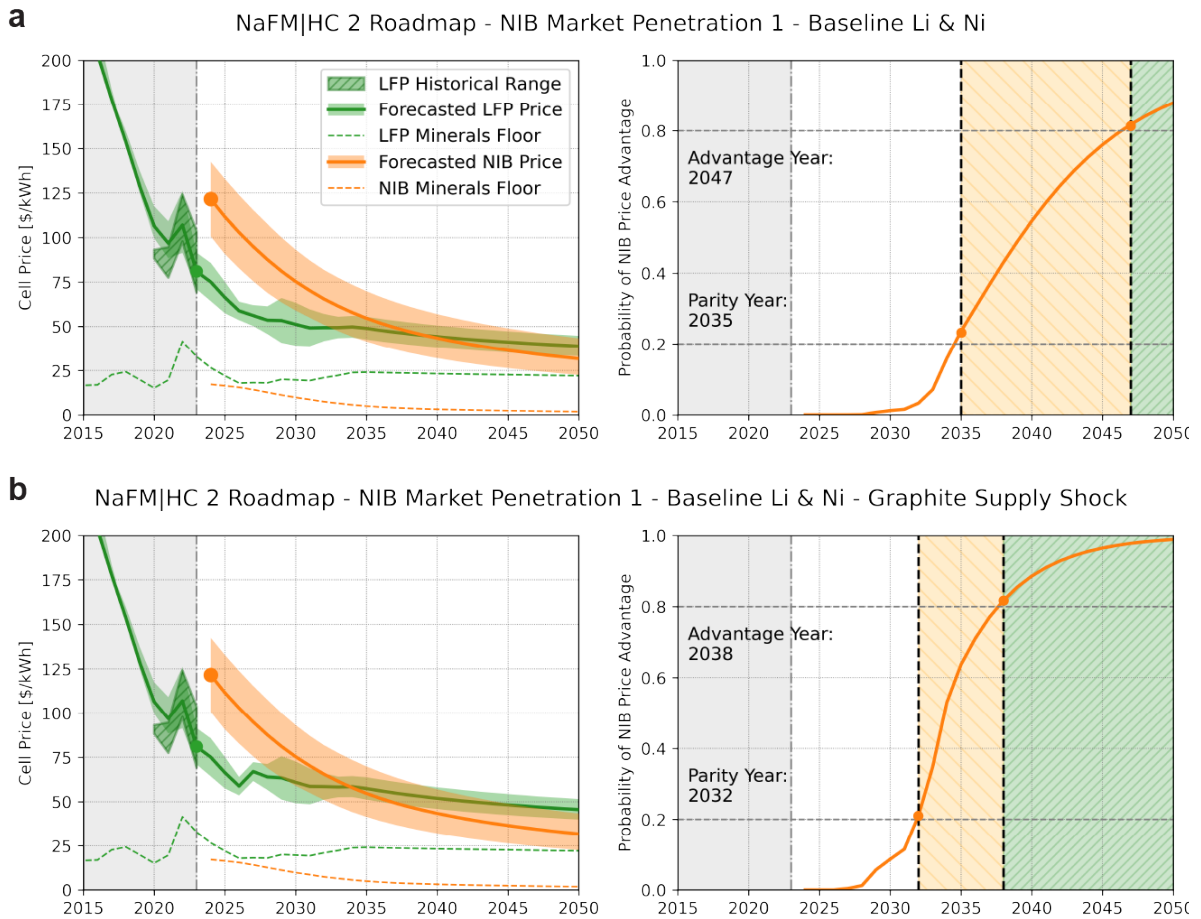


Figure 4: Comparative price curve assessments to evaluate techno-economic competitiveness considering hypothetical Li-ion supply chain disruptions. Example of Roadmap “NaFM|HC 2” with a conservative market penetration (NIB Market Penetration 1), baseline lithium and nickel prices, and **a.** no graphite supply shock or **b.** a hypothetical graphite supply shock in 2027. Comparative price curves (left) and probability profiles (right) allow evaluation of Price Parity and Price Advantage timelines. The example shown in **b** has a 4-year timeframe (yellow hatched) where Na-ion and LFP are closely competitive, whereas the example in **a** has a 12-year competitive timeframe.

Discussion / Conclusions

Our scenarios modeling reveal key trends in the conditions enabling maximum Na-ion techno-economic competitiveness. Figure 5 shows a clustered plot of all 6,048 scenarios categorized by gravimetric energy density and supply chain conditions, where a strong dependence on both factors reasonably describes the modeled timelines to Na-ion Price Advantage over LFP. When supply chain conditions are unfavorable for Li-ion (specifically LFP)—such as high lithium prices, graphite supply shocks, or both—Na-ion competitiveness is accelerated across the board. In contrast, when supply chain conditions are unfavorable for Na-ion (specifically nickel-containing chemistries), competitiveness is significantly hindered. As indicated by the trends from left to right, pursuing technology development roadmaps that maximize energy densities is important to accelerate timelines to competitiveness. Note that a large subset (2,522) of scenarios do not produce conditions for Na-ion Price Advantage before 2050, represented by the open circles in Figure 5. Importantly, however, this does not mean Na-ion is not competitive. A similar clustered plot as Figure 5 in Supplementary Discussion 13.1 shows the timelines to Na-ion Price Parity with LFP, illustrating that over 40% of all modeled scenarios reach a Price Parity condition on or before 2030, and the average “parity period” spans 5.6 ± 3.6 years. With Na-ion being a competitive, viable substitute to Li-

ion having similar price curves (assuming performance parity is achieved), any disruptions to the Li-ion supply chain will likely present Na-ion as an immediately price advantageous alternative.

For example, if lithium prices increase between now and 2027 and remain high (~\$50,000 tonne⁻¹ lithium carbonate equivalent [LCE], see Supplementary Discussion 2.1), over 55% of all Na-ion technical roadmaps lead to a Price Advantage condition before 2035. In contrast, if lithium minerals prices remain low (around \$10,000 tonne⁻¹ LCE, see Supplementary Discussion Section 2.1), there will be virtually no Na-ion development scenarios that will result in a Price Advantage condition without a coinciding supply chain disruption in graphite (or potentially other Li-ion specific materials). For reference, the spot price of lithium at the time of this writing (2024) averages \$10,000 – 15,000 tonne⁻¹—the result from oversupply of battery metals due to a slump in electric vehicle sales in the latter half of 2023^{7,34}. Whether lithium prices can continue to stay low is thus a question with profound implications, especially on the competitiveness of Na-ion batteries.

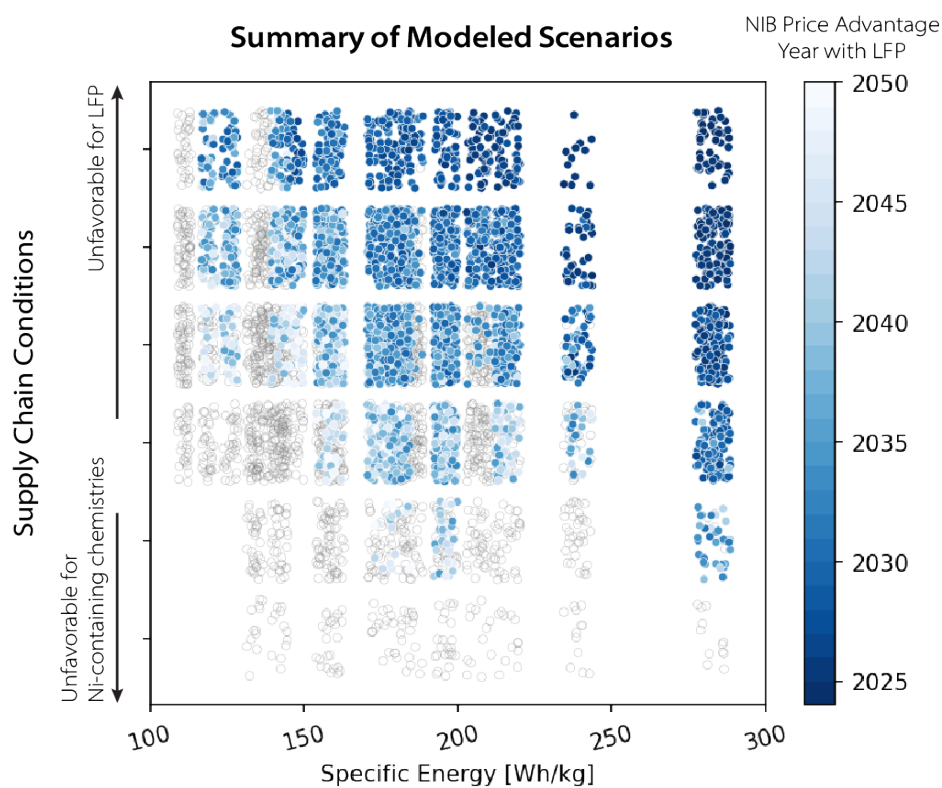


Figure 5: Na-ion techno-economic competitiveness highly dependent on supply chain conditions and technology development roadmaps toward higher energy densities. Heatmap showing timelines to Price Advantage. Supply chain conditions ranked categorically here via summation of integer increments/decrements of lithium, graphite, and nickel supply chain conditions according to Na-ion favorability—with increased nickel commodity pricing being unfavorable to only nickel-containing Na-ion layered oxide cathodes. For example, a high lithium price scenario (+1) coinciding with a graphite supply shock (+1) will produce a supply chain score of +2. The x-axis is ranked by the specific energy density targets achieved by 2030 in the various roadmaps.

The fastest and most certain way for Na-ion to be price advantageous is to reduce materials intensity by increasing materials and cell-level energy densities. This is supported quantitatively in the parameter sensitivity analysis shown in Figure 6, where some of the biggest drivers of forecasted Na-ion cell prices in 2030 and 2040 are accessible upper voltage cutoffs, cathode and anode specific capacities, and electrode thicknesses. Increasing accessible upper voltage cutoffs (a capability specific to layered oxide cathodes with solid-solution intercalation behavior) simultaneously increases available specific capacity and the nominal voltage, which unsurprisingly compounds to provide the largest feature importance. However, this

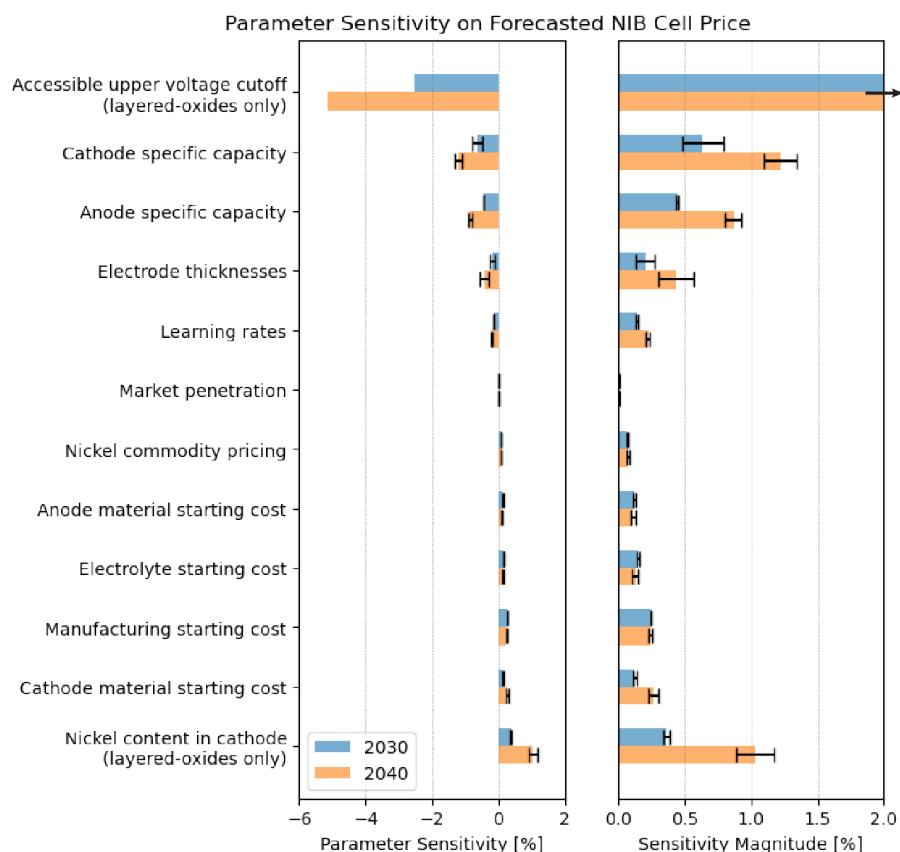


Figure 6: Increasing energy densities and reducing critical minerals content are biggest levers to affect Na-ion cell prices. Parameter sensitivity analysis on the relative importance of features affecting Na-ion cell prices in 2030 (blue) and 2040 (orange). Error bars show standard deviation of parameter sensitivity between multiple one-at-a-time (OAT) perturbations, and the right-hand plot shows the absolute values of parameter sensitivities to enable comparison. Certain features (e.g. reducing nickel content in cathodes and increasing accessible voltage cutoff) are specific to layered oxide cathodes only. A pattern emerges indicating design directions that increase energy densities (accessible voltage, cathode and anode specific capacities, and electrode thicknesses) are key drivers of price. Additionally, the reduction of nickel-content in cathodes has a significant impact on the minerals price floor—more so than the absolute price of nickel commodities. These provide guidance on road mapping directions to maximize the techno-economic competitiveness of Na-ion.

is not always an available option due to material limitations, gas release, or challenges with power electronics upon systems integration (see Supplementary Discussion 7.7)²¹. Therefore, increasing specific capacity alone is an important strategy. In nickel-containing cathodes, this can ideally be done in conjunction with minimizing nickel content due to its relative feature importance.

Increasing the specific capacity of hard carbon anodes is yet another critical design direction identified. With low tap and calender densities, hard carbons impose practical thickness limitations that relegate a balanced cathode to low areal capacity loadings (mAh-cm⁻²). Knock-on effects include requiring more electrolyte volume to saturate increased porosity within electrodes. Additionally, the aggressively slope voltage profiles of hard carbons limits the deliverable cell energy, which negatively impacts cost performance⁴⁴. For these reasons, hard carbons may enable the first generation of Na-ion batteries to demonstrate commercial viability but may require considerable specific capacity improvements (>400 mAh-g⁻¹) or outright replacement to enable long-term techno-economic competitiveness with Li-ion.

Replacing hard carbons with alloying-anodes, such as tin, is one approach to significantly increase anode specific capacity. In our models however, despite a NaNM|Sn baseline cell starting off ~30% lower price than a NaNM|HC cell, its observed price curve appears to fall at a slower rate. This is explained by both

the minerals price floor and engineering design floor of metallic tin both leaving little room for further improvements on cost and material-level performance. Therefore, alloy-based anodes appear to be effective tools to lower costs in the short-term but may require cathode improvements to stay competitive in the long-term.

An alternative design direction is to forgo an anode material altogether and opt for an anode-free cell configuration. This of course would require higher-risk innovation but may not require substantial improvements to current-generation Na-ion cathode technology. Roadmap “NaNM|AF 1”, for example, does not assume any improvements to cathode specific capacity and only assumes an increase in areal capacity loadings of state-of-art nickel-based layered oxides while maintaining a modest upper cutoff voltage of 4.0V. However, advanced separators, electrolytes, and/or current collectors required to enable anode-free designs must do so without reversing the techno-economic argument. Here, we highlight the importance of using such a techno-economic toolkit to *drive* research decision making as opposed to applying it *post facto*.

Finally, despite NFPP cathodes being less than half the cost of NNM and exhibiting a low minerals floor, the confluence of three technical parameters—low specific capacity, low tap density, and low voltage—present challenges to outright advantage on a \$-kWh⁻¹ basis. Its volumetric capacity (mAh-cm⁻³) is even lower than that of hard carbons, which results in low areal capacity loadings. Necessary routes to compete therefore likely require dry electrode processing to enable ultra-thick electrodes and incorporating alloy-based anodes to increase energy density. However, we again note that cell-level prices do not adequately capture other critical performance features, and NFPP-based Na-ion cells may prove more competitive at the systems-level if safety, thermal robustness, and cycle life metrics can be demonstrated to exceed those of LFP.

Both Figure 5 and Figure 6 illustrate that technical development roadmaps are not only beneficial but imperative to Na-ion’s techno-economic competitiveness. Relying solely on learning-by-doing from scale is insufficient to compete with the rapidly evolving Li-ion trends. Therefore, adjusting between the most conservative and aggressive market penetration scenarios yielded minimal feature importance on future Na-ion prices. Similarly, adjusting learning rates to higher-than-typical (“Aggressive”) values of 20 ± 3% for the Na-ion cathode, anode, and electrolyte also had modest feature importance. These observations suggest that engineering advancements are a greater lever to affect prices than the limited room for materials price reductions via learning-by-doing. This increases the likelihood of competitiveness, as price reductions do not rely on a chicken-and-egg problem with capturing market share. Another way to interpret this result is that government intervention may be better allocated by investing in R&D as opposed to subsidizing (or mandating) adoption.

In closing, Na-ion deserves significant research, development, and commercialization attention. We caution against assumptions and promises of immediate or near-term (pre-2030) price advantage against Li-ion, specifically LFP, but believe it has a critical role to play in the energy transition as a viably scalable Li-ion substitute under circumstances of supply chain volatility. Therefore, we believe investing in Na-ion development roadmaps to maintain a competitive track with Li-ion would be prudent. In the same vein, investments in Li-ion supply chain security should not be foregone given the demonstrated sensitivity to supply shocks.

The ultimate objective of developing low-cost batteries is to enable rapid deployment of energy storage in vehicular and stationary applications to meet the needs of the energy transition. These goals must be met even in the face of rising geopolitical tensions and supply chain volatilities. It is therefore not only important to accurately forecast price trends for incumbent technologies, but also critical to understand competitive or substitutional opportunities for emerging technologies. Our proposed modeling framework herein enables such an approach. Modeled outcomes help guide research endeavors and inform strategic investments commensurate with the probability of techno-economic competitiveness and commercial success.

Methods.

Componential floor-constrained learning curves. The typical Wright's learning curve follows the form:

$$Y = Ax^{-b} \quad (1)$$

where the price of a technology Y at a given cumulative experience x is described by the price of the first unit A and a rate of price reduction b . Here, the Learning Rate (or Experience Rate) is defined as the percentage price reduction after every doubling of cumulative experience, given by:

$$\text{LR} = 1 - 2^{-b} \quad (2)$$

As established above, these curves have been demonstrated to accurately capture the price trends across various sectors in a technology-agnostic manner, but they can also overestimate price reductions when technologies approach their price floors dictated by physical limits. In such scenarios, the equation can be modified to incorporate a floor constraint, shown by:

$$Y = (A_0 - A_{\text{floor},0}) \left(\frac{x_t}{x_0} \right)^{-b} + A_{\text{floor},t} \quad (3)$$

Here $A_{\text{floor},0}$ and $A_{\text{floor},t}$ illustrate that the price floors can evolve dynamically with time. Cumulative experience is also normalized for a more practical implementation of the general form in (1) that enables one to use the known price and cumulative ‘‘incurred’’ experience of components in the present and backcast and forecast accordingly. It also enables us to use actual quantities produced (in kT or Mm², for example) in fitting historical data where such production data is available, and switch to using anticipated demand (in GWh) in projecting future price trends. Agreement on present pricing is therefore all that is required to yield continuity between historical and forecasted prices. In this paper, we implement dynamically varying minerals price floors obtained from historical and forecasted price trends to capture the price evolution of individual component costs of a battery. This enables us to capture individual learning rates, market growth rates, and price floors between material components, which are unlikely to always be the same. This is represented in general form as:

$$Y_{\text{cell}} = \left(\sum_n^k M_{n,t} \times \left[(a_{n_0} - a_{n_{\text{floor},0}}) \left(\frac{x_{n,t}}{x_{n,0}} \right)^{-b_n} + a_{n_{\text{floor},t}} \right] \right) + a_{\text{mfg}} \left(\frac{x_{\text{mfg},t}}{x_{\text{mfg},0}} \right)^{-b_{\text{mfg}}} \quad (4)$$

The first term of the right-hand-side aggregates the individual material component costs of a battery cell, each defined by its own learning rate, $-b_n$, normalized cumulative experience, $\left(\frac{x_{n,t}}{x_{n,0}} \right)$, price floor, $a_{n_{\text{floor},t}}$, and a material intensity scalar, $M_{n,t}$, that captures the kg-kWh⁻¹ or m²-kWh⁻¹ contribution required for the representative modeled cell design. Here, $n \in$ Positive Active Material, Negative Active Material, Electrolyte, Separator, Positive Current Collector, Negative Current Collector, and Others. While in practice, all material components will have hard physical limits of a price floor, some components have negligible minerals costs, including polyolefins and conductive carbons. Therefore, for those materials, $a_{n_{\text{floor},t}}$ and $a_{n_{\text{floor},0}}$ are zeroed. The second term of the right-hand-side captures the costs associated with manufacturing, including equipment depreciation, labor, scrap, SG&A, other overheads, warranty, and profit. Notably, this second term is an unconstrained learning curve as there is no direct physical basis to institute a hard price floor. One may consider implementing manufacturing CapEx as a potential price floor, but as we do not yet have a clear methodology to firmly establish a minimum, we leave it unconstrained in this paper. The materials intensity scalar is used to capture the improvements to cell design and active materials specific capacities, both of which are key contributors to historic cell price declines. This componential approach captures the nuance that different components of a battery may learn at different rates, experience different market growth scenarios, and be constrained by respectively different floors.

The above learning curves can be correlated with time by defining individual component market growth rates. Here, we use Gompertz sigmoidal functions to describe the annual demand of individual battery components, as they provide better fits to market projections than standard logistic functions¹⁸. The annual production capacity at year t can be defined as:

$$q_{n,t} = q_{n,\text{base}} \exp \left[\ln \left(\frac{q_{n,\text{sat}}}{q_{n,\text{base}}} \right) (1 - \exp[-r_n t]) \right] \quad (5)$$

where $q_{n,\text{base}}$, $q_{n,\text{sat}}$, and r_n represent the starting annual production capacity, the annual production capacity upon market saturation, and growth rate of component n , respectively. Notably, not all battery components experience the same market growth conditions. For example, whereas the demand for graphite materials in tonnes per annum scales closely with the cumulative demand of total Li-ion batteries due to it being the predominant anode chemistry, LFP and NMC materials will each scale at a lower rate due to their fractional market share. With this, the cumulative capacity can be obtained from

$$x_{n,t} = \sum_{t=0}^T q_{n,t} \quad (6)$$

Minerals pricing. Each mineral dataset was converted into aggregate averages with a sample size of $n \geq 3$ if including proprietary industry sources, or $n = 1$ if data was only available from USGS. Due to the proprietary nature of each of the industry-supplied forecasts, the minerals pricing datasets are averaged at each time step with 95% confidence intervals to prevent traceability to any one data source using the formula:

$$\mu \pm 1.96 \frac{\sigma}{\sqrt{n}} \quad (7)$$

While USGS datasets do not provide minerals price forecasts, industry intelligence firms do, and we use their 2023 forecasts as our baseline scenario for the key minerals (lithium, nickel, cobalt, etc.) looking forward. As expected, there is good agreement on historical minerals pricing but notably larger variances between forecasts within the next decade. Due to inherently large uncertainties associated with forecasting prices of volatile minerals, we also perform analysis of self-generated fixed price scenarios (e.g. high/mid/low) on the key commodities to evaluate the sensitivity of outcomes (see Supplementary Discussion 2.1).

Historical material component pricing. All prices obtained from industry and literature were inflation-adjusted to USD2023. For any year with multiple data points, averages and confidence intervals were calculated using the same methodology above. For tabulating annual production quantities (in kT or Mm²), gaps in data were interpolated using the requisite CAGRs established by the bounding years for which data was available, where CAGR is defined by:

$$\text{CAGR} = \left(\frac{P_2}{P_1} \right)^{1/t} - 1 \quad (8)$$

Cell modeling. To accurately model cells, representative half-cell voltage vs. specific capacity (mAh-g⁻¹) curves of positive and anode material candidates (e.g. LFP, NMC622, NMC811, graphite) were extracted from literature and were mathematically scaled to meet target electrode coating mass loadings, active mass fractions, areal capacity loadings, and calender densities (and therefore porosities). Importantly, first cycle (de)lithiation or (de)sodiation curves were utilized in order capture differences in first cycle efficiencies between positive and negative electrode pairings, and full cell voltage curves were obtained by subtracting negative from positive. This approach is critical to obtaining accurate predictions of realizable energy densities⁴⁴. Cell modeling details are discussed at length in Supplementary Discussion 7, along with validation against experimental curves.

Once the electrode balancing procedure is completed to obtain accurate unit cell designs, the electrode parameters were inputted to the Battery Performance and Cost (BatPaC, v5.1) spreadsheet model produced by Argonne National Lab⁴⁵ to obtain exact mass- and areal-quantities per stored energy content (kg-kWh⁻¹ or m²-kWh⁻¹). Additionally, we leverage the detailed manufacturing cost calculations within BatPaC to obtain the present-day manufacturing costs on a per-kWh basis. We take this approach for the following reasons: (1) Despite being highly detailed in modeling manufacturing-related costs, BatPaC has shortcomings in capturing the true voltage, capacity, and energy characteristics of cells due to inherent limitations of a spreadsheet approach. Especially considering occasional mismatched first cycle efficiencies between cathode and anode pairings and uniquely sloped or stepped voltage curves of emerging Na-ion materials, the true energy (Wh)—which is the area underneath the voltage curve between capacity and voltage windows—can often be miscalculated. This may result in errors in calculating true \$-kWh⁻¹⁴⁴. (2) We note that BatPaC only models large format (>60 Ah) pouch cells, whereas some of the cells modeled (e.g. Tesla 4680 cylindrical cells) do not share the same format. However, we replicate all cell designs using BatPaC to enable systematic comparisons across generations and chemistries, and we also note that materials intensity, energy densities, and manufacturing costs at GWh scale will not deviate substantially between formats. This general approach allows us to systematically evaluate new cell designs and obtain cell manufacturing costs associated with each design while being more nuanced in electrode balancing. See Supplementary Discussion 15 for details on BatPaC Modifications made in our modeling efforts.

Roadmap modeling. To capture the evolution of technical advancements within cell engineering that has contributed substantially to the price declines observed through time, we assign each of the cell designs modeled in Supplementary Discussion 7 to a particular year that represents the requisite technological progress. Then, based upon the differences in the material intensities for each component (in kg-kWh⁻¹ or m²-kWh⁻¹), we fit a curve with an asymptotic limit defined by practical theoretical or engineering limits. The curve follows the form:

$$M = M_{\min} + Ae^{-b*(t-t_0)} \quad (9)$$

where M_{\min} is defined by Equations (11) – (16) for each material component. Note that this can be considered a modified form of Moore's Law. Here, the cathode and anode minimum materials intensities are defined by their respective maximum theoretical specific capacities and allowable electrode thicknesses. The minimum electrolyte materials intensity is defined by the total pore volume within the electrodes only. The minimum separator materials intensity (in m²-kWh⁻¹) is defined by a maximum cathode thickness and therefore capacity loading. The minimum positive and negative current collector materials intensities are then calculated from the separator materials intensity but converted to a mass-basis (kg-kWh⁻¹) based upon the densities and minimum practical thicknesses of the foils. For the Other material components category, the asymptotic limit M_{\min} is omitted as there is no basis for a minimum limit. In a similar fashion, the maximum theoretical cell-level specific energy is calculated by summing up a

balanced anode- or cathode-limited unit-cell based on the provided limits, where Equation (9) is modified to approach an asymptotic maximum as opposed to a minimum, with the form:

$$SE = SE_{\max} - Ae^{-b*(t-t_0)} \quad (10)$$

The equations defining the calculation of minimum materials intensities is as follows:

$$M_{\text{CAT}_{\text{theo}}} \left[\frac{\text{kg}}{\text{kWh}} \right] = \frac{1}{q_{\text{CAT}_{\text{theo}}}} \left[\frac{\text{g}}{\text{mAh}} \right] * \frac{1}{E_{\text{cell}}} \left[\frac{1}{\text{V}} \right] \quad (11)$$

$$M_{\text{AND}_{\text{theo}}} \left[\frac{\text{kg}}{\text{kWh}} \right] = \frac{1}{q_{\text{AND}_{\text{theo}}}} \left[\frac{\text{g}}{\text{mAh}} \right] * \frac{1}{E_{\text{cell}}} \left[\frac{1}{\text{V}} \right] \quad (12)$$

$$M_{\text{ELY}_{\text{theo}}} \left[\frac{\text{kg}}{\text{kWh}} \right] = \rho_{\text{ELY}} \left[\frac{\text{g}}{\text{cm}^3} \right] * \left\{ \frac{\varepsilon_{\text{CAT}_{\text{min}}} [\%]}{\rho_{\text{CAT}_{\text{theo}}} \left[\frac{\text{g}}{\text{cm}^3} \right] * q_{\text{CAT}_{\text{theo}}} \left[\frac{\text{mAh}}{\text{g}} \right]} + NP_Ratio * \frac{\varepsilon_{\text{AND}_{\text{min}}} [\%]}{\rho_{\text{AND}_{\text{theo}}} \left[\frac{\text{g}}{\text{cm}^3} \right] * q_{\text{AND}_{\text{theo}}} \left[\frac{\text{mAh}}{\text{g}} \right]} \right\} * \frac{1}{E_{\text{cell}}} \left[\frac{1}{\text{V}} \right] \quad (13)$$

$$M_{\text{SEP}_{\text{theo}}} \left[\frac{\text{m}^2}{\text{kWh}} \right] = \frac{2}{t_{\text{CAT}_{\text{max}}} [\mu\text{m}] * \rho_{\text{CAT}_{\text{theo}}} \left[\frac{\text{g}}{\text{cm}^3} \right] * q_{\text{CAT}_{\text{theo}}} \left[\frac{\text{mAh}}{\text{g}} \right] * (1 - \varepsilon_{\text{CAT}_{\text{min}}} [\%])} * \frac{1}{E_{\text{cell}}} \left[\frac{1}{\text{V}} \right] \quad (14)$$

$$M_{\text{PCC}_{\text{theo}}} \left[\frac{\text{kg}}{\text{kWh}} \right] = M_{\text{SEP}_{\text{theo}}} \left[\frac{\text{m}^2}{\text{kWh}} \right] * \rho_{\text{PCC}_{\text{theo}}} \left[\frac{\text{g}}{\text{cm}^3} \right] * t_{\text{PCC}_{\text{min}}} [\mu\text{m}] \quad (15)$$

$$M_{\text{NCC}_{\text{theo}}} \left[\frac{\text{kg}}{\text{kWh}} \right] = M_{\text{SEP}_{\text{theo}}} \left[\frac{\text{m}^2}{\text{kWh}} \right] * \rho_{\text{NCC}_{\text{theo}}} \left[\frac{\text{g}}{\text{cm}^3} \right] * t_{\text{NCC}_{\text{min}}} [\mu\text{m}] \quad (16)$$

For each component, the A and b parameters in Equation (9) are fitted after the M_{\min} parameter is calculated. Occasionally, when one parameter is assumed to not experience significant improvements, such as the specific capacity of graphite (current values $\sim 360 \text{ mAh-g}^{-1}$ are already near the theoretical capacity), the fitted parameter b may end up < 0 , making the exponential term > 0 with a very shallow slope. This is an artifact of fitting, and we do not expect actual material performance to decline with time. Therefore, in cases where the fitted b parameter ends up negative, we instead use a flat line with zero slope centered at the average of the fitted values.

REFERENCES

1. *Electric Vehicle & Battery Supply Chain - Strategic Planning Outlook to 2050*. (2023).
2. Pillot, C. *The Rechargeable Battery Market and Main Trends 2022-2030*. (2023).
3. Lithium-ion Battery Pack Prices Rise for First Time to an Average of \$151/kWh. *BloombergNEF* <https://about.bnef.com/blog/lithium-ion-battery-pack-prices-rise-for-first-time-to-an-average-of-151-kwh/> (2022).
4. Ziegler, M. S. & Trancik, J. E. Re-examining rates of lithium-ion battery technology improvement and cost decline. *Energy Environ. Sci.* **14**, 1635–1651 (2021).
5. Ziegler, M. S., Song, J. & Trancik, J. E. Determinants of lithium-ion battery technology cost decline. *Energy Environ. Sci.* **14**, 6074–6098 (2021).
6. *Benchmark Cell Prices Assessment*. (2024).
7. Khan, Y. Low Battery Metal Prices Set to Persist in 2024, Adding Friction to Energy Transition. *The Wall Street Journal* (2023).
8. Stoikou, E. Battery Prices Are Falling Again as Raw Material Costs Drop. *Bloomberg* (2023).
9. Lee, A. Nickel Price Crash Seen Extending Indonesia's Grip on Supply. *Bloomberg* (2024).
10. McNulty, R. & Williams, E. OPINION: Why sodium ion batteries will take longer than people think. *Benchmark Source* <https://source.benchmarkminerals.com/article/opinion-why-sodium-ion-batteries-will-take-longer-than-people-think>.
11. Wright, T. P. Factors Affecting the Cost of Airplanes. *J. Aeronaut. Sci.* **3**, 122–128 (1936).
12. Nagy, B., Farmer, J. D., Bui, Q. M. & Trancik, J. E. Statistical Basis for Predicting Technological Progress. *PLOS ONE* **8**, e52669 (2013).
13. Schmidt, O., Melchior, S., Hawkes, A. & Staffell, I. Projecting the Future Levelized Cost of Electricity Storage Technologies. *Joule* **3**, 81–100 (2019).
14. Schmidt, O., Hawkes, A., Gambhir, A. & Staffell, I. The future cost of electrical energy storage based on experience rates. *Nat. Energy* **2**, 1–8 (2017).
15. Frith, J. T., Lacey, M. J. & Ulissi, U. A non-academic perspective on the future of lithium-based batteries. *Nat. Commun.* **14**, 420 (2023).
16. Nykvist, B. & Nilsson, M. Rapidly falling costs of battery packs for electric vehicles. *Nat. Clim. Change* **5**, 329–332 (2015).
17. Kittner, N., Lill, F. & Kammen, D. M. Energy storage deployment and innovation for the clean energy transition. *Nat. Energy* **2**, 1–6 (2017).
18. Hsieh, I.-Y. L., Pan, M. S., Chiang, Y.-M. & Green, W. H. Learning only buys you so much: Practical limits on battery price reduction. *Appl. Energy* **239**, 218–224 (2019).
19. Wang, A. & Yiu, N. *Battery Component Price Report December 2023*. (2023).
20. Jephcott, B. Sodium-ion Battery Market Research Report. *Hong Kong*.
21. Barker, J. *et al.* Industry Expert Panel.
22. *Minerals Price Forecasts*. (2024).
23. *Battery Materials Pricing Data*.
24. *Mineral Commodity Summaries*. <https://www.usgs.gov/centers/national-minerals-information-center/mineral-commodity-summaries>.
25. *Anode Prices*. (2024).
26. *Cathode Prices*. (2024).
27. Stock, S. *et al.* Cell teardown and characterization of an automotive prismatic LFP battery. *Electrochimica Acta* **471**, 143341 (2023).
28. Ank, M. *et al.* Lithium-Ion Cells in Automotive Applications: Tesla 4680 Cylindrical Cell Teardown and Characterization. *J. Electrochem. Soc.* **170**, 120536 (2023).
29. Günter, F. J. & Wassiliadis, N. State of the Art of Lithium-Ion Pouch Cells in Automotive Applications: Cell Teardown and Characterization. *J. Electrochem. Soc.* **169**, 030515 (2022).
30. Barnett, B. & Llc, T. PHEV Battery Cost Assessment. (2010).
31. Gallagher, K. G. & Nelson, P. A. 6 - Manufacturing Costs of Batteries for Electric Vehicles. in *Lithium-Ion Batteries* (ed. Pistoia, G.) 97–126 (Elsevier, Amsterdam, 2014). doi:10.1016/B978-0-444-59513-3.00006-6.
32. Lain, M. J., Brandon, J. & Kendrick, E. Design Strategies for High Power vs. High Energy Lithium Ion Cells. *Batteries* **5**, 64 (2019).
33. Levine, S. The Electric: China Digs In With Iron-Based Batteries, Wrong-Footing Western Automakers. *The Information* (2024).
34. Liu, S. & Patton, D. China lithium price poised for further decline in 2024 -analysts. *Reuters* (2023).
35. Tarascon, J.-M. Na-ion versus Li-ion Batteries: Complementarity Rather than Competitiveness. *Joule* **4**, 1616–1620 (2020).
36. Xu, Z.-L. *et al.* Tailoring sodium intercalation in graphite for high energy and power sodium ion batteries. *Nat. Commun.* **10**, 2598 (2019).

37. Zhang, B. *et al.* Microsized Sn as Advanced Anodes in Glyme-Based Electrolyte for Na-Ion Batteries. *Adv. Mater.* **28**, 9824–9830 (2016).
38. Yang, T., Luo, D., Liu, Y., Yu, A. & Chen, Z. Anode-free sodium metal batteries as rising stars for lithium-ion alternatives. *iScience* **26**, 105982 (2023).
39. Chen, Y. *et al.* Prospects for practical anode-free sodium batteries. *Mater. Today* (2024) doi:10.1016/j.mattod.2024.01.002.
40. Rudola, A. *et al.* Commercialisation of high energy density sodium-ion batteries: Faradion's journey and outlook. *J. Mater. Chem. A* **9**, 8279–8302 (2021).
41. Barker, J. The Path to the Successful Commercialization of Sodium-Ion Batteries. (2022).
42. Rudola, A., Sayers, R., Wright, C. J. & Barker, J. Opportunities for moderate-range electric vehicles using sustainable sodium-ion batteries. *Nat. Energy* **8**, 215–218 (2023).
43. Farmer, J. D. & Lafond, F. How predictable is technological progress? *Res. Policy* **45**, 647–665 (2016).
44. Innocenti, A., Beringer, S. & Passerini, S. Cost and performance analysis as a valuable tool for battery material research. *Nat. Rev. Mater.* 1–11 (2024) doi:10.1038/s41578-024-00657-2.
45. Knehr, K. W., Kubal, J. J., Nelson, P. A. & Ahmed, S. Battery Performance and Cost (BatPaC) v5.1 Spreadsheet Model. Chemical Sciences and Engineering Division Argonne National Lab (2022).

Acknowledgements

This work was supported by three offices within the U.S. Department of Energy through the STEER Program, a partnership between the SLAC-Stanford Battery Center and the Stanford Precourt Institute for Energy. Specifically, the three offices are: the Office of Electricity, the Vehicle Technologies Office under the Office of Energy Efficiency & Renewable Energy, and the Office of Technology Transitions. Additionally, this work was supported in part by the National Science Foundation Graduate Research Fellowship Program (award number DGE-2146755).

The authors thank the panel of industry consultants/experts cited throughout the work, including those that provided written feedback/critique of the manuscript draft (Supplementary Discussion 16). They include: Jerry Barker, Colin Wessells (Natron Energy), Brandon Kelly (Peak Energy), Spencer Gore (Bedrock Materials), Andrew Wang, Darren Tan (Unigrid), Linda Jing (Tesla), Tyler Evans (Mana Battery), Nicholas Singstock (Mana Battery), Heather A.S. Platt (Mana Battery), Katherine He (TDK Ventures), Fabrice Renard (Avicenne Energy), Christophe Pillot (Avicenne Energy), Wayne Yen (LongTime Technologies), William Hwang (LongTime Technologies), Kara Rodby (Volta Energy Technologies), Simon Lux (Universität Münster), Jannis Wesselkämper (Universität Münster), Philipp Voß (Universität Münster), Charlie Parker (Ratel Consulting), Mrigi Munjal (MIT), the Boston Consulting Group, and Brian Spatocco (Lucid Motors). The written feedback/critique from those that consented to our publishing is included in the Supplementary Information.

The authors further thank those attendees who attended the Na-ion Commercialization Forum hosted by STEER on April 15th, 2024 on Stanford University campus centered around the pre-print of this manuscript. All discussions were held under Chatham House Rule with productive discussions that led to important revisions for this work. A summary of the key learnings from the Forum are included in Supplementary Discussion 17.

The authors finally thank Karan Bhuwalka, Hari Ramachandran, Julia Frohmann, and Alexis Geslin for their thoughtful comments and feedback on the manuscripts. The authors especially thank Karan Bhuwalka and Hari Ramachandran for collecting formal responses and summarizing learnings from the STEER Commercialization Forum.

Author Contributions

Adrian Yao: conceptualization, methodology, modeling, data gathering, data contributor relations, data curation, analysis, visualization, writing, project administration, funding acquisition. **Sally Benson:** conceptualization, resources, review, editing, supervision, funding acquisition. **William Chueh:** conceptualization, resources, review, editing, supervision, funding acquisition.

Declarations of Interests

A.Y. is among the founders of EnPower, a manufacturer of Li-ion batteries. W.C.C. is among the founders of Mitra Chem, a developer of LFP cathode materials.

Supplementary Information

Supplementary Information to this work is available and attached separately.